THE JOURNAL OF BIOLOGICAL CHEMISTRY VOL. 289, NO. 37, pp. 25976–25986, September 12, 2014

Adropin Is a Brain Membrane-bound Protein Regulating Physical Activity via the NB-3/Notch Signaling Pathway in Mice*

Received for publication, April 25, 2014, and in revised form, July 14, 2014 Published, JBC Papers in Press, July 29, 2014, DOI 10.1074/jbc.M114.576058

Chi-Ming Wong[‡§¶1,2], **Yudong Wang**[‡§1], **Jimmy Tsz Hang Lee**[‡§], **Zhe Huang**[‡§], **Donghai Wu**[‖], **Aimin Xu**[‡§¶**3], **and Karen Siu Ling Lam**[‡§¶]

From the [‡]*State Key Laboratory of Pharmaceutical Biotechnology,* [§]*Department of Medicine,* [**]*Department of Pharmacology and Pharmacy,* [¶]*Research Centre of Heart, Brain, Hormone and Healthy Aging, Li Ka Shing Faculty of Medicine, The University of Hong Kong and the* [‖]*Guangzhou Institutes of Biomedicine and Health, Hong Kong, China*

Background: The mechanism of action of adropin on metabolism remains elusive.
Results: Adropin is a plasma membrane protein that can bind to the brain-specific, non-canonical Notch1 ligand NB-3.
Conclusion: Adropin regulates physical activity, motor coordination, and cerebellum development in mice via the NB-3/Notch1 signaling pathway.
Significance: Adropin is a highly conserved polypeptide that might also be important for cerebellum development in mammals.

Adropin is a highly conserved polypeptide that has been suggested to act as an endocrine factor that plays important roles in metabolic regulation, insulin sensitivity, and endothelial functions. However, in this study, we provide evidence demonstrating that adropin is a plasma membrane protein expressed abundantly in the brain. Using a yeast two-hybrid screening approach, we identified NB-3/Contactin 6, a brain-specific, non-canonical, membrane-tethered Notch1 ligand, as an interaction partner of adropin. Furthermore, this interaction promotes NB3-induced activation of Notch signaling and the expression of Notch target genes. We also generated and characterized adropin knockout mice to explore the role of adropin *in vivo*. Adropin knockout mice exhibited decreased locomotor activity and impaired motor coordination coupled with defective synapse formation, a phenotype similar to NB-3 knockout mice. Taken together, our data suggest that adropin is a membrane-bound protein that interacts with the brain-specific Notch1 ligand NB3. It regulates physical activity and motor coordination via the NB-3/Notch signaling pathway and plays an important role in cerebellum development in mice.

Adropin, composed of 76 amino acids, is encoded by the energy homeostasis-associated (Enho) gene that is remarkably down-regulated in the livers of mice with high fat diet-induced obesity or genetic obesity because of melanocortin receptor deficiency ($Mc3r^{-/-}$) or leptin deficiency. It was initially identified on microarray screening for genes that were up-regulated or down-regulated in $Mc3r^{-/-}$ mice (1). The expression of hepatic Enho mRNA is tightly regulated by energy intake in mice (1). Transgenic overexpression or synthetic adropin treatment in diet-induced obesity mice attenuated hepatosteatosis and insulin resistance (1), whereas global adropin knockout (adrKO)[4] mice, generated by the same group of researchers, were associated with increased hepatosteatosis, adiposity, and insulin resistance (2). In addition, adropin has been found to have a protective effect on endothelial function in the mouse (3). However, because the beneficial effects of adropin against hepatosteatosis and hyperinsulinemia associated with obesity and endothelial dysfunction in mice were determined on the basis of a single publication, most of the findings remain to be validated.

Interestingly, human and murine adropin share identical amino acid sequences. Correlations between circulating adropin levels and different pathophysiological states in mice and humans have been reported (1–14). In brief, the circulating concentration of adropin was reduced markedly in several metabolic diseases, including obesity-associated insulin resistance (1, 5, 11); obesity-related, nonalcoholic fatty liver disease (11); gestational diabetes mellitus (7); and endothelial dysfunction (6, 8, 14). However, conversely, other studies found that plasma adropin levels in humans were not correlated inversely with obesity on the basis of body mass index (6, 8, 13) or with endothelial dysfunction (9). In addition, unlike findings in mice, plasma adropin levels in humans do not change in response to fasting and refeeding (5).

Although previous studies suggest a role of adropin as a possible metabolic regulator, the underlying molecular mechanism

* This work was supported by RGC Collaborative Research Fund Grant HKU2/CRF/12R, matching funds from the University of Hong Kong for the State Key Laboratory of Pharmaceutical Biotechnology, and by National 973 Basic Research Program of China (2011CB504004 and 2010CB945500).
[1] Both authors contributed equally to this work.
[2] To whom correspondence may be addressed: Dept. of Medicine, Li Ka Shing Faculty of Medicine, The University of Hong Kong, 21 Sassoon Rd., Pokfulam, Hong Kong, China. Tel.: 852-3917-9747; Fax: 852-2816-2095; E-mail: wispwong@hku.hk.
[3] To whom correspondence may be addressed: Dept. of Medicine, Li Ka Shing Faculty of Medicine, The University of Hong Kong, 21 Sassoon Rd., Pokfulam, Hong Kong, China. Tel.: 852-3917-9754; Fax: 852-2816-2095; E-mail: amxu@hkucc.hku.hk.

[4] The abbreviations used are: adrKO, adropin KO; HFD, high-fat diet; CLAMS, comprehensive laboratory animal monitoring system; TRITC, tetramethylrhodamine isothiocyanate; qPCR, quantitative PCR; BD, binding domain; AD, activation domain; F-Luc, firefly luciferase; R-Luc, *Renilla* luciferase; DAPT, *N*-[*N*-(3,5-difluorophenacetyl)-L-alanyl]-*S*-phenylglycine *t*-butyl ester.

for the actions of adropin remains elusive at this stage. Published works have mainly focused on studying the action of adropin on the liver, white adipose tissue, and endothelium (1–3). However, on the basis of the mRNA expression profiles of adropin, it is expressed most abundantly in the brain in both mice and humans (15), whereas the central action of adropin has not been investigated. In this study, we characterized the expression and biochemical properties of adropin and investigated the central action of adropin in the mouse.

EXPERIMENTAL PROCEDURES

Cells and Plasmid Constructs

HEK293 and HeLa cells were obtained from the ATCC. Cells were maintained in DMEM supplemented with 10% fetal bovine serum (Invitrogen) and 1% penicillin/streptomycin in a humidified atmosphere of 5% CO_2 at 37 °C. The ORF for adropin used in this study was obtained from the C57BL/6 wild-type mouse liver cDNA. To isolate the cDNA fragment that contains the full-length adropin protein coding sequence, PCRs using primers (forward, 5′gaa ttc *gcc acc* atg ggg gca gcc atc tcc 3′; reverse, 5′gga tcc tta *ctt atc gtc gtc atc ctt gta atc* ggg ctg cag cag gta gct gcc 3′) were performed. After PCR, the DNA fragment was digested with restriction enzymes (EcoRI and BamHI) and inserted into the pcDNA3.1 vector (Invitrogen) for transient expression in mammalian cells. To clone the DNA fragment encoding adropin protein (C-terminal, amino acids 30–76) for yeast two-hybrid screening, oligonucleotide primers (forward, 5′gaa ttc tgc cat tct cga tct gct gac gtc 3′; reverse, 5′gga tcc tta ggg ctg cag cag gta gct gcc 3′) were used to perform PCR. After PCR, the DNA fragment was digested with restriction enzymes (EcoRI and BamHI) and inserted into the pGBKT7 vector (Clontech) for transient expression in yeast. All expression plasmids were verified by sequencing. The jetPEI *in vitro* transfection reagent (Polyplus) was used to transfect DNA into HEK293 and HeLa cells following the instructions of the manufacturer.

Generation of Anti-adropin Antibody

A His-tagged cDNA fragment encoding mouse adropin (amino acid residues 30–76) was subcloned into the pROEX-HTb vector, which was then used to transform into host *Escherichia coli* BL21 cells. Oligonucleotide primers (forward, 5′gga tcc *atg cat cat cac cat cac cac* tgc cat tct cga tct gct gac gtc3′; reverse, 5′gaa ttc *tta* ggg ctg cag cag gta gct gcc 3′) were used to perform PCR. The expression was induced by addition of 1 mM isopropyl 1-thio-β-D-galactopyranoside. His-tagged adropin fragment was purified from the bacterial lysates using a nickel-nitrilotriacetic acid-agarose column as described previously (16). The purity of the protein was confirmed by SDS-PAGE and HPLC. The polyclonal antibody against the recombinant mouse adropin was raised in female New Zealand White rabbits as described previously (16). The specificity of the antibodies was verified by Western blotting.

Generation of Mice with Targeted Disruption of Adropin

The adrKO targeting vector was designed to disrupt the expression of adropin by inserting a neomycin resistance gene into the 5′ region of the adropin open reading frame in the adropin gene. The targeting vector was linearized and electroporated into 129Sv/J-derived CJ7 ES cells. The neomycin-resistant clones were identified by PCR, and correct ES cell clones were microinjected into the blastocyst stage of C57BL/6 embryos to generate chimeric mice that were subsequently backcrossed with C57BL/6 mice to generate F1 animals heterozygous for the mutated *adropin* allele. The offspring was routinely genotyped by PCR using 35 cycles of 95 °C for 30 s, 55 °C for 30 s, and 72 °C for 45 s with the following primers: 5′ ATG GTT GGC CAC CCC AGA 3′ (forward) and 5′ ACT AGT GAG ACG TGC TAC TTC 3′ (reverse). AdrKO mice were generated by the Shanghai Research Center for Model Organisms.

Animal Maintenance

All animal experimental procedures were approved by the Committee on the Use of Live Animals for Teaching and Research of the University of Hong Kong and were carried out in accordance with the Guide for the Care and Use of Laboratory Animals. AdrKO mice were backcrossed onto a C57BL/6 genetic background for at least six generations before investigation. AdrKO mice and WT littermates were housed in a 12-h light/dark cycle (07:00–19:00) room under controlled temperatures (23 ± 1 °C) with free access to water and standard chow (20% kcal protein, 10% kcal fat, and 70% kcal carbohydrates) or high-fat diet (HFD; Research Diet; 20% kcal protein, 45% kcal fat, and 35% kcal carbohydrates), respectively. Mice were sacrificed by cardiac puncture at the indicated time points. Serum and tissues were collected for further analysis.

Indirect Calorimetry and Body Composition

Energy expenditure was measured using the comprehensive laboratory animal monitoring system (CLAMS, Columbus Instruments, Columbus, OH) as described previously (17, 18). Briefly, mice were housed singly in CLAMS cages and acclimated for 48 h, and then data on oxygen consumption (VO_2), carbon dioxide consumption (VCO_2), respiratory exchange ratio (VCO_2/VO_2), food intake, and locomotor activity were recorded simultaneously for a further 72 h. Body composition (fat mass and lean mass) was measured using ^1H magnetic resonance spectroscopy (Bruker BioSpin, Billerica, MA) as described previously (19).

Glucose Homeostasis

Glucose homeostasis was assessed in standard chow- or HFD-fed AdrKO mice and their WT littermates. Intraperitoneal glucose tolerance tests were performed at 10:00 a.m. in mice fasted for 16 h using a blood glucose meter (Accu-CHEK Advantage, Roche) to detect glucose levels in the blood sampled from the tail vein after intraperitoneal injection of D-glucose (Sigma-Aldrich, St. Louis, MO) (1 g/kg of body weight). 20 μl of blood samples were collected at 0, 30, 60, and 90 min for insulin ELISA (Antibody and Immunoassay Services, The University of Hong Kong). For insulin tolerance tests, a similar procedure was followed, except that mice were fasted for 6 h, and insulin (Eli Lilly and Co., Indianapolis, LN) (1 unit/kg of body weight) was injected intraperitoneally.

Behavior Analysis

Rotarod Test—Mice were placed on a horizontally oriented, rotating rod (20 rpm/min). The length of time (latency) that a given mouse stayed on the rotating rod was recorded, and the maximum time was set to 180 s.

Wheel Running Test—Mice were housed singly in standard cages equipped with running wheels (Lafayette Instruments) with food and water *ad libitum* and with a 12-h light/12-h dark cycle for 10 days. Wheel revolution counts were recorded automatically by computer.

Hanging Wire Test—Four paws were placed onto a metal wire by handling the tail. When the mouse had grasped the wire, it was gently turned upside-down to face upward, and its tail was released. The time until the mouse fell to the floor was recorded, and the maximum time was set to 120 s.

RNA Extraction and Real-time PCR

Total RNA was extracted from various mouse tissues with TRIzol reagent (Invitrogen), and treated with RNase-free DNase (Promega, Madison, WI) at 37 °C for 30 min to remove genomic DNA. For reverse transcription, 1 μg of the total RNA was converted to first-strand complementary DNA in 20 μl reactions using a cDNA synthesis kit (Promega). Quantitative real-time PCR was performed in duplicate in a total reaction volume of 20 μl with SYBR Green PCR Master Mix (Qiagen, Hilden, Germany) in an ABI Prism 7000 instrument (Applied Biosystems) with the following parameters: 95°C for 5 min, followed by 40 two-step cycles at 95 °C for 10 s and 60 °C for 30 s. The forward and reverse primers used for PCR amplification of mouse *HES1*, *HES5*, *HEY1*, *Cdkn1a*, β-actin, and GAPDH were as follows: *HES1*, 5′-CAG CCA GTG TCA ACA CGA CAC-3′ (forward) and 5′-TCG TTC ATG CAC TCG CTG AG-3′ (reverse); *HES5*, 5′-CGC ATC AAC AGC AGC ATA GAG-3′ (forward) and 5′-TGG AAG TGG TAA AGC AGC TTC-3′ (reverse); *HEY1*, 5′-CAC GCC ACT ATG CTC AAT GT-3′ (forward) and 5′-TCT CCC TTC ACC TCA CTG CT-3′ (reverse); *Cdkn1a*, 5′-CTT GCA CTC TGG TGT CTG AG-3′ (forward) and 5′-GCA CTT CAG GGT TTT CTC TTG-3′ (reverse); GAPDH, 5′-CTT TGT CAA GCT CAT TTC CTG G-3′ (forward) and 5′-TCT TGC TCA GTG TCC TTG C-3′ (reverse); and β-actin 5′-CTA AGG CCA ACC GTG AAA G-3′ (forward) and 5′-ACC AGA GGC ATA CAG GGA CA-3′ (reverse). Analysis was performed with ABI Prism 7000 SDS software, and the mRNA expression of each gene was calculated after being normalized with β-actin expression using the comparative Ct method.

Yeast Two-hybrid Assay

The C-terminus of mouse adropin (amino acids 30–76) was used for yeast two-hybrid screening. The screening procedures were conducted following the instructions of the manufacturer. The cDNA library used for this screening was a universal mouse (normalized) library (catalog no. 630482, Clontech). About 1 million cotransformants were screened for the four reporter genes *HIS*, *lacZ*, *ADE*, and *AUR1-C* on plates containing the respective selective medium.

Western Blotting and Cellular Fractionation

Cells were lysed in radioimmune precipitation assay buffer (50 mM Tris-Cl, 150 mM NaCl, 1% Nonidet P-40, 0.5% sodium deoxycholate, and 0.1% SDS), and total protein concentration was quantified by Bradford assay. Equal amounts of cellular protein were separated by SDS-PAGE, and immunoblotting was carried out as described previously (17, 19). For subcellular fractionation, the Qproteome plasma membrane kit (Qiagen) was used according to the protocol of the manufacturer.

Coimmunoprecipitation

HEK293 cells were transfected with pcDNA3.1-adropin-FLAG and/or pcDNA3.1-NB3-HA. Their lysate (200 μg of protein) was incubated with 50 μl of anti-FLAG M2 affinity bead (Sigma-Aldrich). The beads were washed with PBST (100 mM sodium phosphate, 150 mM NaCl, 0.1% Triton X-100, pH 7.2). The immobilized immune complexes were then collected from the lysate and analyzed by Western blotting with indicated antibodies.

Immunofluorescence

HeLa cells grown on coverslips were transfected with pcDNA3.1-adropin. After 72 h, cells were fixed with 4% paraformaldehyde in PBS and permeabilized with 0.2% Triton X-100. The coverslips were blocked with 5% BSA in PBS for 1 h at 37 °C and incubated with anti-adropin in a 1:50 dilution. Mouse monoclonal anti-cadherin antibody (Affinity Bioreagents) and rabbit anti-FLAG (Sigma-Aldrich) were used for immunostaining. TRITC (red)-conjugated goat anti-mouse and FITC (green)-conjugated goat anti-rabbit antibodies were used for visualization with a confocal microscope.

Luciferase Reporter Assay

Transfections were done in 6-cm plates (5×10^5 cells/plate), and the cells were harvested after 48 h and lysed in a cell lysis buffer (Promega). Luciferase activity was measured using a luciferase reporter assay system (Promega), and readings were taken on a luminometer.

Statistical Analysis

All experiments were performed using male mice in cohorts consisting of 6–10 mice with data presented as mean ± S.E. Statistical significance was determined by one- or two-way analysis of variance or Student's *t* test, where appropriate, using the Statistical Package for Social Sciences version 16.0 (SPSS, Chicago, IL). In all statistical comparisons, $p < 0.05$ was used to indicate a significant difference.

RESULTS

Adropin Is a Membrane-bound Protein Highly Expressed in the Brain—Quantitative PCR (qPCR) analysis showed that the expression of adropin mRNA is highest in the brain, followed by the liver (Fig. 1*A*; 6-fold higher in the brain than in the liver), which is in agreement with a previous study (1) and the gene expression database Expression Atlas (15). To further explore the tissue distribution of the adropin protein, we generated a specific antibody against adropin for Western blot analysis

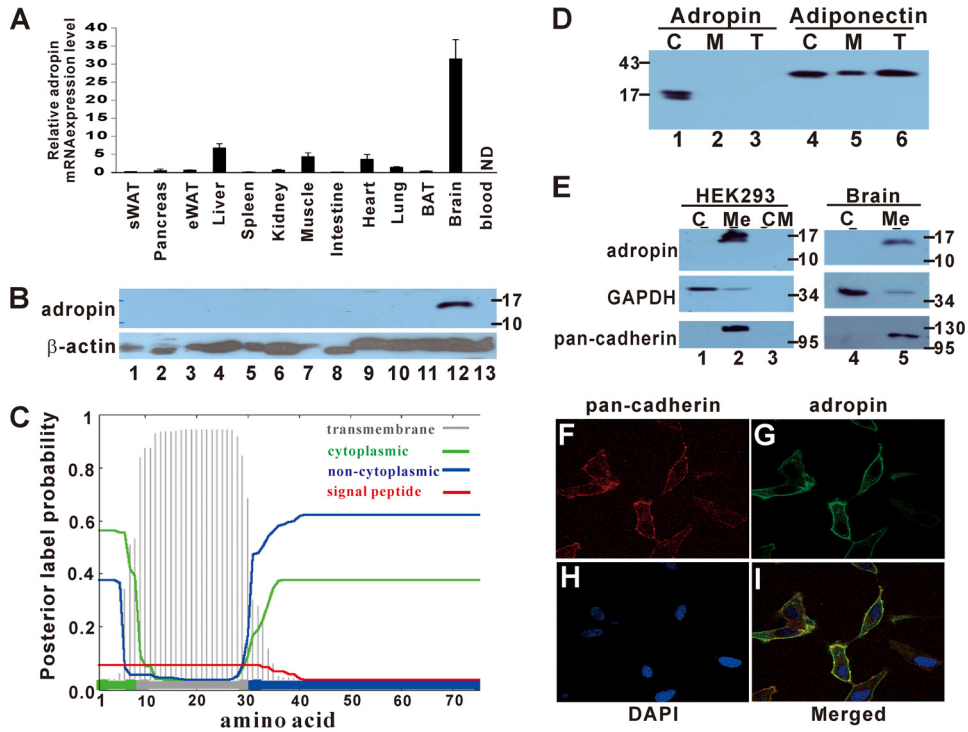

FIGURE 1. **Adropin is a brain plasma membrane-bound protein.** *A* and *B*, qPCR and Western blotting to check the mRNA (*A*) and protein (*B*) levels of adropin in different tissues of 8-week-old male C57BL/6N mice. In *B*, the arrangement of the samples is the same as in *A*. *sWAT*, subcutaneous white adipose tissue; *eWAT*, epididymal white adipose tissue; *BAT*, brown adipose tissue. *C*, the subcellular localization of adropin was predicted by the Phobius program. On the basis of the analysis, for the N-terminal from amino acids 1–9, because the probability of cytoplasmic is higher than the non-cytoplasmic, this region should be localized in the cytoplasm. From amino acids 9–30, the score for the transmembrane is the highest (>0.9) among all four possibilities, so this region was suggested to be the transmembrane domain. For the C-terminal from amino acids 30–76, because the probability of "non-cytoplasm" is highest, it should be localized outside of the surface of the plasma membrane. The score for the probability of the N-terminal amino acids from 1–33 as a signal peptide is lower than 0.1. *D*, Western blotting of adropin and adiponectin (a secretory protein used as a control) in HEK293 cells. *C*, cell lysate; *M*, culture medium; *T*, concentrated protein by TCA precipitation (4×) of the culture medium. *E*, subcellular fractionation of overexpressed adropin in HEK293 cells and endogenous adropin in mouse brain tissue. *C*, cytosol; *Me*, membrane; *CM*, culture medium. *F–I*, adropin is localized mainly on the plasma membrane. HeLa cells were grown on cover slips and transfected with a plasmid expressing adropin. After 24-h transfection, cells were fixed with 4% paraformaldehyde and stained with anti-pan-cadherin and anti-adropin antibodies. The immunofluorescence analysis was performed by confocal microscopy. Endogenous pan-cadherin (membrane marker) was visualized in *red* (*F*), adropin in green (*G*), and DNA in blue (*H*). *I*, colocalization of adropin and pan-cadherin was detected as yellow fluorescence.

when the same amount of protein was loaded (Fig. 1*B*). Because adropin had been proposed as a hepatocyte-secreted protein (1), it was expected that adropin could be found in the liver and blood samples. The controversial findings regarding circulating adropin (6, 8, 9, 13) led us to reinvestigate the biochemical properties of adropin.

First, prediction of transmembrane topology and the signal peptide of adropin were performed by bioinformatics analysis, including Phobius and Signal IP 4.1 (20, 21). From amino acids 9–30, the score for the transmembrane was highest (>0.9). Among all four possibilities, Phobius predicted this region to be a transmembrane domain (Fig. 1*C*). This may be due to the fact that this region is enriched in hydrophobic residues (including seven leucine, three isoleucine, and three valine residues of 21 amino acids) with a very poorly defined protease cleavage site (20–23).

To verify the bioinformatics-based prediction, *in vitro* experiments were performed to examine the presence and location of adropin in HEK293 cells harboring the plasmid overexpressing adropin. To our surprise, no adropin was detected in the conditioned medium (Fig. 1*D*, *lane 2*), even in the sample concentrated 4-fold by TCA precipitation (Fig. 1*D*, *lane 3*). The adropin protein was only detected in total cell lysates (Fig. 1*D*, *lane 1*). As a comparison, adiponectin, a well known antidiabetic hormone secreted from fat cells (24), was detected in both the cell lysates and the conditioned culture medium (Fig. 1*D*, *lanes 4* and *5*) and further enriched by TCA precipitation (Fig. 1*D*, *lane 6*).

Because adropin was detected in cell lysates but not in the conditioned medium, we proceeded to investigate the subcellular localization of adropin. Subcellular protein fractionation analysis with transfected HEK293 cells overexpressing adropin was performed, and the selected fractions were examined by Western blotting (Fig. 1*E*, *left panel*). In addition, to prevent the expression level from affecting its subcellular localization, mouse brain lysate for endogenous adropin was used (Fig. 1*E*, *right panel*). Both overexpressed and endogenous adropin were found to cofractionate predominately with the plasma membrane-bound protein pan-cadherin (Fig. 1*E*, *lanes 2* and *5*).

In addition, the membrane marker pan-cadherin was used to examine whether adropin localizes to the plasma membrane by confocal microscopy analysis (Fig. 1, *F–I*). Colocalization of pan-cadherin (stained *red* in Fig. 1*F*) and adropin (stained green in Fig. 1*G*) was detected as yellow fluorescence in Fig. 1*I*. Our data showed that adropin was mainly localized to the plasma membrane (Fig. 1, *F versus G*). The evidence from subcellular protein fractionation and confocal microscopy analysis clearly indicates that adropin is indeed a plasma membrane-bound protein, as predicted by bioinformatics.

Adropin Binds to NB-3 and Activates Notch Signaling in Vitro—Because information about the molecular functions of adropin was scarce, we performed yeast two-hybrid screening to explore the function of adropin via its binding proteins. Because the N-terminal transmembrane domain (amino acids 1–29) of adropin is too hydrophobic, the C terminus of adropin (amino acids 30–76) was used as bait for yeast two-hybrid screening. In line with our finding of adropin as a membrane-bound protein, most of the adropin binding partners identified by this approach were also membrane proteins. Among them, we focused on the prey, neural recognition molecule 3 (NB-3, also known as Cntn6) in this study because NB-3 is a brain-specific glycosylphosphatidylinositol anchor protein (25, 26). To verify the interaction, the plasmid GAL4 DNA-binding domain (GAL4-BD)-fused adropin and/or GAL4 activation domain (GAL4-AD)-fused NB-3 were transformed into the yeast strain Y2HGold (auxotrophic for histidine because the endogenous *HIS3* gene was deleted). Only the yeast cells transformed with both the GAL4-BD-adropin and GAL4-AD-NB-3 plasmids could grow under selective conditions lacking histidine (Fig. 2*A*, *right panel*, *lane 3 versus* lanes *1* and *2*) because the interaction of GAL4-BD-adropin and GAL4-AD-NB-3 drove the transcription of the exogenously introduced Gal4-responsive *HIS3* gene.

The physical interaction of NB-3 and adropin was also validated by coimmunoprecipitation analysis in a mammalian cell culture system. The cell lysates of HEK293 cells overexpressing FLAG-tagged adropin and/or HA-tagged NB-3 were used (Fig. 2*B*). Without FLAG-tagged adropin, the HA-tagged NB-3 could not be pulled down by anti-FLAG beads (Fig. 2*B*, *lane 8*), and all unbounded NB-3 remained in the supernatant (Fig. 2*B*, *lane 9*). However, with FLAG-tagged adropin, NB-3 was found mainly in the pellet fraction (Fig. 2*B*, *lane 5 versus lane 8*) instead of in the supernatant (Fig. 2*B*, *lane 6 versus lane 9*). Our results clearly demonstrate that adropin physically binds to NB-3.

In addition, the colocalization of NB-3 and adropin was confirmed further by confocal microscopy. As shown in Fig. 2*C*, both adropin and NB-3 are colocalized to the plasma membrane. In addition, we also performed coimmunoprecipitation to confirm that endogenous adropin binds to NB-3 in mouse brain samples. As shown in Fig. 2*D*, in brain tissue lysate from WT mice, both the adropin and NB-3 proteins were enriched in the pulldown samples (Fig. 2*D*, *lane 3*). However, in the lysate from adrKO mice, because there is no adropin protein in the lysate (Fig. 2*D*, *lane 2*), no NB-3 was pulled down (Fig. 2*D*, *lane 4*). These data suggest that endogenous NB-3 and adropin interact with each other.

NB-3 functions as a membrane-tethered Notch1 ligand and belongs to the contactin family that mediates cell surface interaction during nervous system development (27). NB-3 promotes Notch1 activation and, subsequently, drives the expression of Notch1 target genes such as *HES1* and *HEY1* (28, 29). To decipher the effects of adropin on NB-3-mediated Notch1 signaling, adropin and/or NB-3 were overexpressed in HEK293 cells harboring both a firefly luciferase (*F-Luc*) reporter driven by the *HES1* promoter and a *Renilla* luciferase (*R-Luc*) reporter with the CMV promoter as an internal control. As shown in Fig. 2*E*, overexpressing the Notch1 ligand NB-3 could induce the expression of *HES1-F-Luc* (28). Furthermore, NB-3 and adropin apparently synergized with each other to further increase the activity of the *HES1* promoter.

The induction of expression of the endogenous *HES1* and *HEY1* mRNA levels was also examined by qPCR. Overexpressing both NB-3 and adropin in 3T3L1 cells could induce the expression of *HES1* and *HEY1* mRNA (Fig. 2*F*). To further verify that the activation of the transcription of *HES1* and *HEY1* is through the Notch signaling pathway, cells transfected with adropin- and NB-3-overexpressing plasmids were treated with the γ-secretase inhibitor *N*-[*N*-(3,5-difluorophenacetyl)-L-alanyl]-*S*-phenylglycine t-butyl ester (DAPT), where γ-secretase is an enzyme required for Notch activation. As shown in Fig. 2*F*, the induction of both *HES1* and *HEY1* mRNA expression by adropin and NB-3 could be repressed by treatment with the DAPT. Interestingly, it is not necessary to express both adropin and NB-3 in the same cell to activate the Notch signaling pathway. Cocultured cells expressing either adropin or NB-3 could also induce the expression of *HES1* and *HEY1*, and their expression levels were similar to cells transfected with both adropin- and NB-3-overexpressing plasmids. This may be due to the fact that NB-3 is a lipid-anchored protein covalently attached to a fatty acid that serves to anchor NB-3 to the cell membrane face, and it has been reported that the glycophosphatidylinositol anchor NB-3 protein could be transferred intercellularly from one cell to another by a process termed "cell painting" (30).

Generation of Adropin Knockout Mice—To further explore the role of adropin in Notch/NB-3 signaling *in vivo*, we generated adrKO mice to determine its physiological role. As mentioned in a previous study (2), the *adropin* gene comprises two exons, and its ORF is located in exon 2, which overlaps with exon 20 of the adjacent gene dynein, axonemal, intermediate chain 1 (*Dnaic1*) (Fig. 3*A*). To minimize the adverse effect on the expression of *Dnaic1* by disrupting transcription termination sites and/or 3′UTR of *Dnaic1* located on the exon 2 of *adropin* gene, DNA sequence of Neomycin resistance gene (*NEO*) and 126 bp (including the loxP recombination site) were inserted into the 5′ and the 3′ region of the *adropin* ORF, respectively (Fig. 3*A*, *lower panel*), to disrupt the translation of adropin protein. No DNA sequence in the exon 2 of adropin gene was deleted.

The relative position of the primers for the genotyping is shown in Fig. 3*A*, and a typical genotyping result is shown in Fig. 3*B*. RT-PCR was performed to ensure that there were no changes in the expression of *Dnaic1* and *adropin* mRNAs in both WT and adrKO mice (Fig. 3*C*). Because of the insertion of the *NEO* gene into the 5′ region of the adropin ORF, no adropin protein was translated from this bicistronic mRNA. As expected, in our Western blot analysis (Fig. 3*D*), no adropin protein was detected in the brain tissues of adrKO mice.

AdrKO Mice Have Defects in Physical Activity—After successfully obtaining the adrKO mouse line, we further examined its phenotype. The body weight and adiposity of the adrKO mice were similar to WT littermates under both standard chow conditions and after chronic HFD treatment (Fig. 3, *E* and *F*). No significant changes in glucose tolerance and insulin sensitivity were observed by glucose tolerance test and insulin tolerance test, respectively (Fig. 3, *G–I*). Because adropin is highly expressed in the brain (Fig. 1) and binds to NB-3 (Fig. 2), which is important for brain development and motor coordination

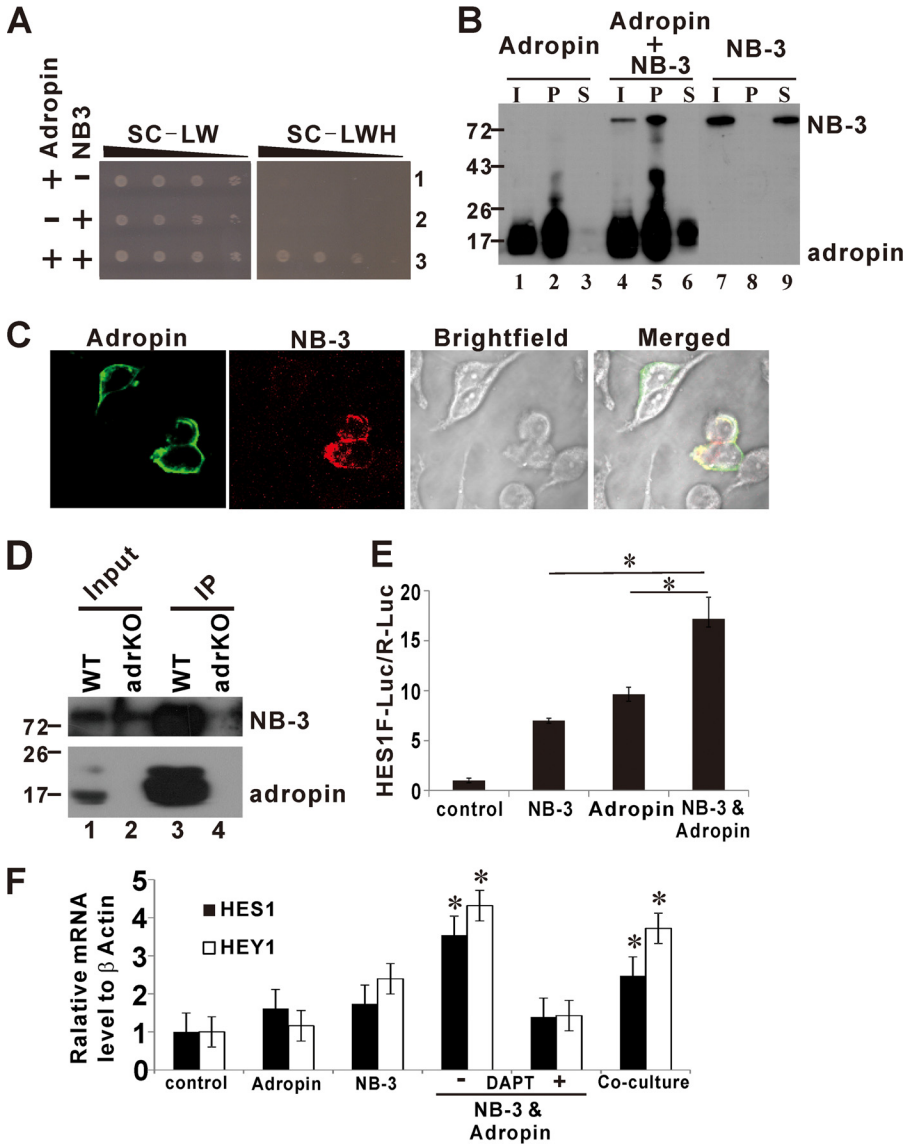

FIGURE 2. **Adropin can bind to NB-3 and modulate the Notch1 signaling pathway.** *A*, validation of the interaction between NB-3 and adropin by yeast two-hybrid assay. Yeast (Y2HGold, Clontech) cells expressing both GAL-BD-adropin and GAL-AD-NB-3 could grow on the selective medium without leucine, tryptophan, and histidine (*LWH*) but not cells expressing either GAL-BD-adropin or GAL-AD-NB-3. *SC*, synthetic complete. *B*, validation of the interaction of NB-3 and adropin by coimmunoprecipitation. FLAG-tagged adropin and/or HA-tagged NB-3 were expressed in HEK293 cells. Immunoprecipitation was performed with anti-FLAG beads, and precipitates were immunoblotted with anti-NB-3 or anti-adropin antibody. *I*, input; *P*, pellet; *S*, supernatant. *C*, confirmation of plasma membrane colocalization of both NB-3 and adropin. HeLa cells were grown on coverslips and transfected with adropin- and NB-3-overexpressing plasmids. After 24-h transfection, cells were fixed with 4% paraformaldehyde and stained with anti-NB-3 and anti-adropin antibodies. Immunofluorescence analysis was performed by confocal microscopy. Adropin is shown in *green* (*first panel*), and NB-3was visualized in red (*second panel*). Colocalization of adropin and NB-3 was detected as *yellow* fluorescence (*third panel*) with bright field images to show where the cells are localized. *D*, validation of the interaction of endogenous adropin and NB-3 by mouse brain tissue samples. Brains from 8-week-old WT and adrKO mice were used. Coimmunoprecipitation was performed with anti-adropin antibody, and precipitates were immunoblotted with either anti-NB-3 or anti-adropin antibodies. *E* and *F*, adropin can induce the expression of Notch-regulating genes. *E*, HEK239 cells were transfected with the *HES1* F-Luc reporter plasmid with NB-3 and/or adropin. The readings were normalized with CMV-R-Luc. The empty vector pcDNA3.1 was used, and corrected luciferase values were arbitrarily set to a value of 1 and served as a reference for comparison of fold differences. *Error bars* indicate mean ± S.D. of triplicate experiments. *, $p < 0.05$. *F*, qPCR was performed to check the mRNA expression levels of *HES1* and *HEY1* mRNA. 3T3L1 cells were transfected with NB-3- and/or adropin-overexpressing plasmid. The empty vector pcDNA3.1 was used as control and served as a reference (set to a value of 1) for comparison of fold differences. We also checked whether cocultured 3T3L1 cells transfected with NB-3- or adropin-overexpressing plasmid could induce the expression of *HES1* and *HEY* mRNA. The γ-secretase inhibitor DAPT was used to inhibit the Notch signaling pathway. Cells were treated with 1 μM DAPT for 24 h before being harvested. *Error bars* indicate mean ± S.D. of triplicate experiments. *, $p < 0.05$ compared with control.

(25), we next investigated whether adropin regulates physical activity via the central nervous system. CLAMS was used to monitor the motor performance of adrKO mice. A significant reduction in locomotor activity (Fig. 4*A*) and a slight decrease in food intake (Fig. 4*B*) were observed in adrKO mice compared with their WT littermates, especially during the dark period. The phenotype of reduced physical activity of our adrKO mice was consistent with the findings of a previous study (2).

To further confirm the physically inactive phenotype of adrKO mice, voluntary wheel running experiments were performed to monitor the movement of the mice for 7 days. The results showed that the running distance of the adrKO mice was significantly less than that of their WT littermates from days 4–7 (Fig. 4*C*). In addition, the locomotor activity of adrKO mice was significantly less than that of their WT littermates in the dark phase (Fig. 4*D*). This may be due to the fact that mice are usually more active in feeding

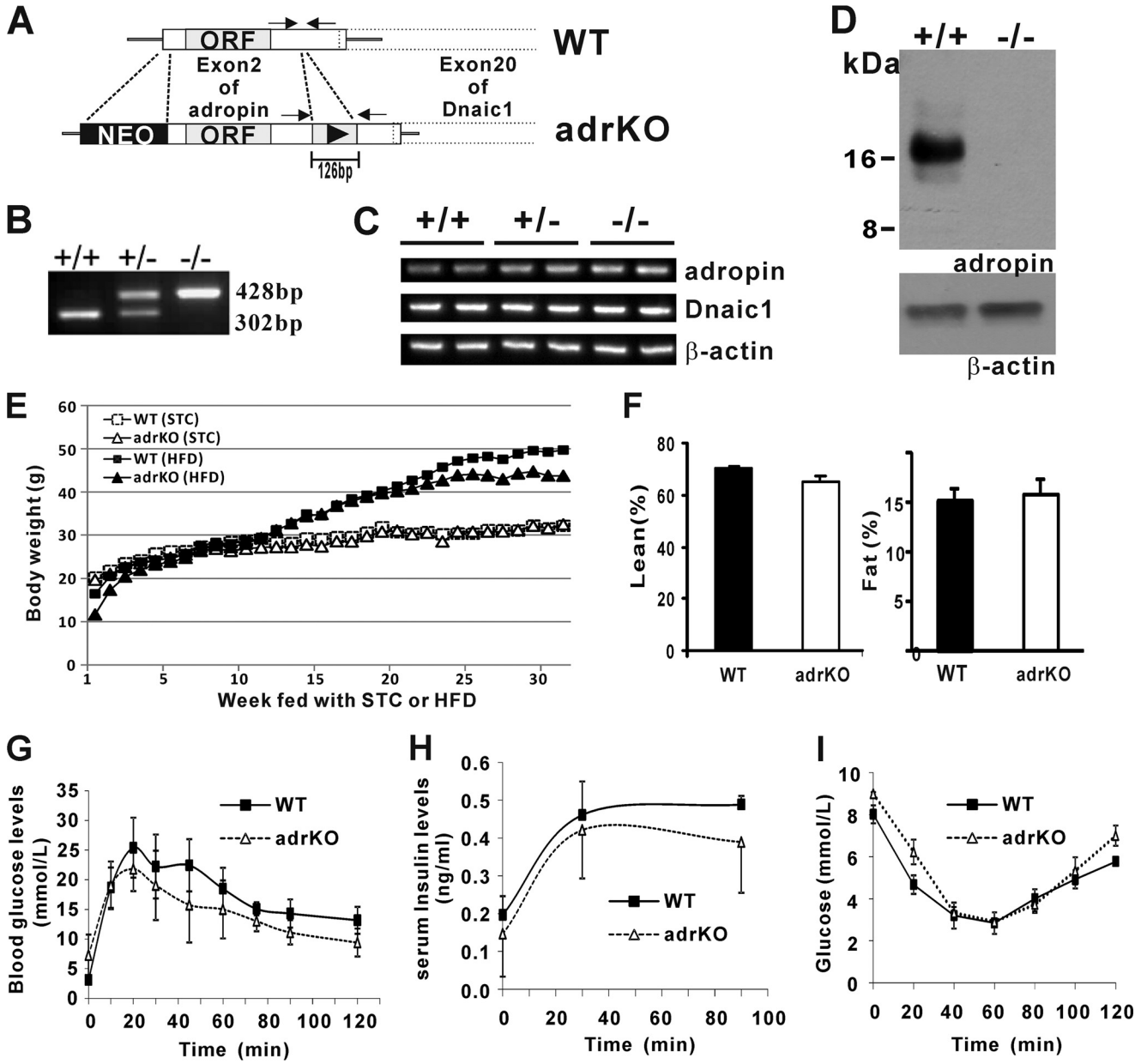

FIGURE 3. **Generation and phenotypic characterization of adrKO mice.** *A*, schematic showing adropin exon 2 of WT and adrKO mice. The *open box* represents exon 2 of *adropin*, the *gray box* represents the *adropin* ORF, the *black box* represents the *neomycin* gene, the *open box with the dashed outline* represents exon 20 of *Dnaic1*, and the *black triangle* represents the loxP recombination site. The *horizontal arrows* represent the primers for genotyping in *B*. *B*, genotyping of WT and adrKO mice by PCR. *C*, RT-PCR was performed to check the mRNA expression level of *adropin* and *Dnaic1*. 1 μg of total RNA samples from the brain of 8-week-old male WT and adrKO mice was used. RT-PCR demonstrated that the expression of adropin and *Dnaic1* mRNAs was not affected in the brain tissues of adrKO mice. *D*, Western blotting of adropin protein in the brains of WT and adrKO mice. No adropin protein was detected in the brain tissue sample of adrKO mice. 100 μg of protein samples from the brains of 8-week-old male WT and adrKO mice were used. Also shown is a comparison of body weight (*E*), fat mass at week 24 of HFD treatment (*F*), glucose tolerance test (*G*), circulating insulin at week 20 of HFD treatment (*H*), and insulin tolerance test at week 24 of HFD treatment (*I*) between WT and adrKO mice ($n = 10–12$ for each group).

and movement during the dark phase, so that the changes became more obvious. In summary, adrKO mice were less active than their WT littermates in the dark phase.

To explore whether the reduction of physical activity in adrKO mice is due to a decrease in muscle strength and/or endurance capacity, forced treadmill running tests were performed (31). There was a significant increase in time (Fig. 4*E*) and number (Fig. 4*F*) of shocks for adrKO mice compared with their WT littermates. Furthermore, the total run distance in adrKO mice was reduced significantly compared with wild-type littermates (Fig. 4*G*). To further examine the possible defects in muscle strength, hanging wire tests were performed. No significant change in the latency of fall between WT and adrKO mice was observed (Fig. 4*H*).

Deletion of Adropin Impairs Motor Coordination and Synapse Formation in the Cerebellum—Because a previous study demonstrated that NB-3 knockout (nb-3KO) mice exhibited impaired motor coordination (32), rotarod tests were performed to evaluate the motor coordination of our adrKO mice. WT mice had a significant improvement in the latency to fall

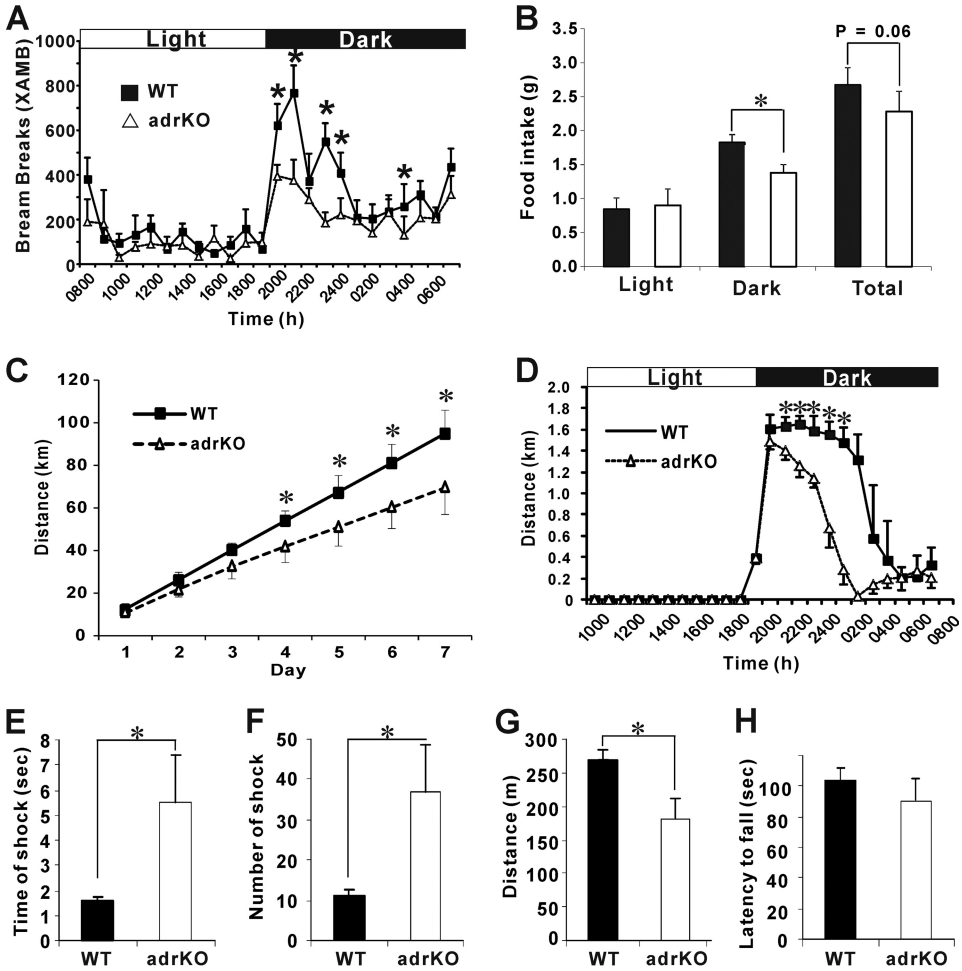

FIGURE 4. **Physical activity is decreased in adrKO mice.** *A* and *B*, basal locomotor activity (*A*) and food intake (*B*) of adrKO mice detected with CLAMS cages. *XAMB*, ambulatory movement on the *x* axis. *C* and *D*, the wheel running test was used to demonstrate that adrKO mice have a physical inactivity phenotype. *C*, accumulated running distance of WT and adrKO mice. *D*, average run speed for WT and adrKO mice at day 7. *E–G*, forced treadmill running tests measured endurance capacity. There were significant increases in time (*E*) and number of shocks (*F*) for adrKO mice compared with their WT littermates, and there was a significant reduction in total distance run by adrKO mice (*G*). *H*, hanging wire test to evaluate muscle strength. There was no significant change in the latency of fall between WT and adrKO mice ($p > 0.05$). Male mice at 8–12 weeks of age were used ($n = 10–12$ for each group). All displayed values are mean ± S.E. *, $p < 0.05$.

after 13 trials (Fig. 5*A*, *black columns*), but adrKO mice were inferior to WT mice in their ability to walk on the rotating rod (Fig. 5*A*, *white versus black columns*), indicating that adrKO mice were impaired in balance control. The poor motor coordination phenotype of adrKO mice matched the respective phenotype in nb-3KO mice reported previously (25). The coordination defect of adrKO mice could also explain their poor performance in the forced treadmill running tests (Fig. 4, *E* and *F*).

Next, we explored whether the deletion of adropin would affect cerebellum development, as observed in nb3-KO mice (27, 33). No gross abnormality in the brain architecture of adrKO mice was observed (data not shown). Then we examined the expression level of NB-3 in the cerebellum of adrKO mice. There was a modest but significant decrease (~15%) in the expression level of NB-3 in the cerebellum of adrKO mice compared with the WT controls (Fig. 5*B*, *left panel*, *top*, *lanes 3* and *4 versus lanes 1* and *2*, $p < 0.05$). Previous studies suggested that NB-3 plays a role in synaptic formation in the developing cerebellum (33), possibly through the Notch1 signaling pathway (28, 29, 34, 35). Therefore, we also measured the expression level of Notch1 in the cerebellum of adrKO mice by Western blot analysis. A modest increase (~20%) in the level of Notch1 in the cerebellum of adrKO mice was observed compared with WT littermates (Fig. 5*B*, *left panel*). In line with the findings, the basal expression levels of the Notch1-regulated genes *HES1*, *HES5*, and *Cdkn1a* were down-regulated in the brain tissue samples of adrKO mice as determined by qPCR (Fig. 5*C*, $p < 0.05$).

A previous study suggested that the impairment of motor coordination in nb-3KO mouse was due to a reduction in synaptic density between Purkinje cells and granule cells located along parallel fibers in the cerebellum of nb-3KO mice (27) because Purkinje cell-granule cell parallel fiber synaptic transmission mediated by the neurotransmitter glutamate is critical for normal cerebellar function, including motor control (36). Therefore, we also measured the synaptic density via the vesicular glutamate transporter (VGlut1)-positive area in the cerebellum of adrKO and WT mice by immunohistochemistry (Fig. 5*D*). Calbindin was used as a marker of Purkinje cells. The den-

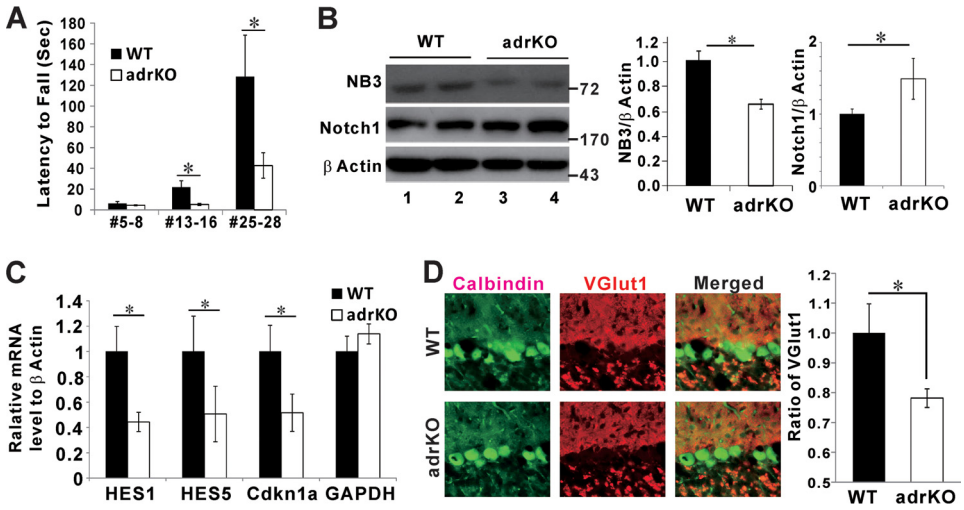

FIGURE 5. **Impaired motor coordination and cerebellar synapse formation in adrKO mice.** *A*, the rotarod test was used to assess motor coordination and balance. The latency time indicates how long mice were able to walk on an accelerating rotarod at speeds from 20 rpm. The adrKO mice had a motor coordination defect. The difference was more significant after the mice were given training with more than 13 trials. Male mice at 8 weeks of age were used (n = 14 per group). *B*, the levels of the endogenous NB-3 and Notch1 in the cerebellum of WT and adrKO mice were examined by Western blotting (*left panel*). Cerebellum were isolated from 8-week-old male WT or adrKO mice, followed by Western blot analysis to detect the expression levels of NB-3 and Notch1. *Right panel*, densitometric analysis for the relative amount of NB-3 ($n = 6$). *, $p < 0.05$. *C*, qPCR to determine the expression levels of *HES1*, *HES5*, *Cdkn1a*, and *GAPDH* mRNA in cerebellum of 8-week-old male WT and adrKO mice. The expression level of β-actin mRNA was used for normalization of the target gene expression levels. The corrected values of WT mice were arbitrarily set to a value of 1 ($n = 5$) *, $p < 0.05$. *D*, cerebellar synaptic defects in adrKO mice. Calbindin was used as a marker of Purkinje cells. VGlut1-positive puncta around Purkinje cells in adrKO and WT mice are shown. The density of the VGlut1 signal was quantified using the JACoP plugin of ImageJ (38). The corrected values of WT mice were arbitrarily set to a value of 1. There was a significant change in the density of VGlut1 puncta in adrKO mice ($n = 6$). *, $p < 0.05$.

sity and number of Purkinje cells in adrKO mice were similar to their WT littermates (Fig. 5*D*, *left panel*, cells stained *green*). However, the density of VGlut1-positive puncta (Fig. 5*D*, *left panel*, cells stained *red*) was decreased slightly but significantly in the cerebellum of adrKO mice ($p < 0.05$) compared with the respective regions of their WT littermates. The observation of the defect in the Purkinje cell synapse is similar to the reported phenotype of nb-3KO mice (27) and could at least partially explain the defects of locomotor activity and coordination in adrKO mice.

DISCUSSION

In this study, we report that adropin is a membrane-anchored protein (Fig. 1). Although several papers published recently have reported that adropin from various mammals could be detected in serum and that its circulating level was altered under different pathophysiological conditions (1–14), we cannot exclude the possibility that a tiny amount of adropin presents in the circulation under certain pathological conditions. Nevertheless, our findings strongly suggest that the majority of adropin protein localizes in the brains of mice and that adropin is in a membrane-bound state under physiological conditions.

To explore the function of adropin *in vivo*, we generated adrKO mice. In agreement with a previous report (2), adrKO mice display reduced physical activity. Our adrKO mice displayed defects in both locomotor activity and coordination. The movement disorders may be due to the decrease in the reduction of NB-3 in the cerebellum and, hence, cerebellar synapse formation in adrKO mice. We hypothesize that adropin binds to a brain-specific membrane-bound protein, NB-3 (Fig. 2, *A–D*), and activates the Notch1 signaling pathway *in vitro*

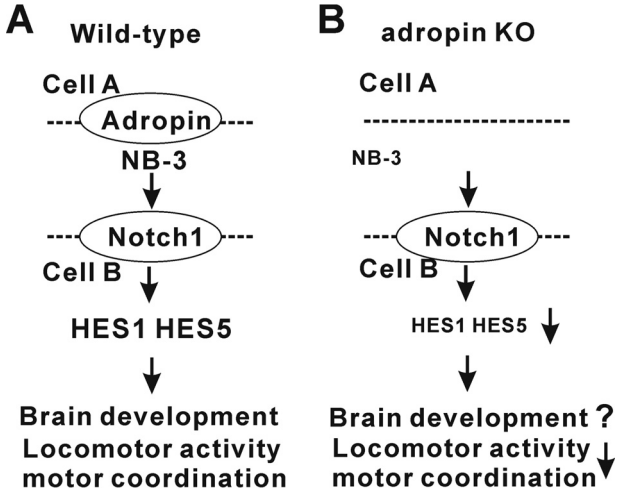

FIGURE 6. **Working model.** *A*, in wild-type mice, adropin cooperates with NB-3 to regulate the Notch1 signaling pathway for normal cerebellar development. Adropin may be important for NB-3 recruitment, enrichment, and/or binding affinity to Notch1 receptor and then affects brain development, locomotor activity, and coordination. *B*, in adropin knockout mice, less NB-3 was recruited, and the Notch1 signaling pathway was repressed. This may affect brain development and, hence, locomotor activity and coordination.

(Fig. 2, *E* and *F*). Because NB-3 is required for normal cerebellum development in mice, we predict that the phenotype of impaired motor activity (Fig. 4, *A*, *C*, and *G*) and coordination (Fig. 5*A*) in our adrKO mice might be due to defects in the NB-3-mediated Notch1 signaling pathway (Fig. 5*C*) and, hence, granule cell-Purkinje cell synapse formation during cerebellar development (Fig. 5*D*). A previous study has demonstrated that adropin is detected at granular and Purkinje cells in the cerebellum (37). Unfortunately, we could not find a suitable anti-adropin antibody to perform a similar immunohistochemical

study to identify the cell types and precise region(s) in the brain where the adropin protein is expressed.

In conclusion, our data suggest that adropin cooperates with NB-3 to regulate Notch1 signaling in brain development and, hence, the locomotor activity and coordination of mice (Fig. 6). It would be of great interest to further experimentally delineate the exact mechanism underlying how adropin modulates the Notch1 signaling pathway and, hence, brain development via NB-3 *in vivo*. Because the amino acid sequences of human and mouse adropin are identical, the findings of the mouse adropin research will also apply to humans.

Acknowledgments—We thank Prof. Kazutada Watanabe and Yasushi Shimoda for the plasmid overexpressing NB-3 and antibodies against NB-3, Prof. Raphael Kopan for the HES1-luc plasmid, Prof. Sookja Kim Chung and Ang Li for helpful discussions, and laboratory members Drs. Connie Woo, Kenneth Cheng, Ruby Hoo, and Cyrus Chan for critical reading of the manuscript.

REFERENCES

1. Kumar, K. G., Trevaskis, J. L., Lam, D. D., Sutton, G. M., Koza, R. A., Chouljenko, V. N., Kousoulas, K. G., Rogers, P. M., Kesterson, R. A., Thearle, M., Ferrante, A. W., Jr., Mynatt, R. L., Burris, T. P., Dong, J. Z., Halem, H. A., Culler, M. D., Heisler, L. K., Stephens, J. M., and Butler, A. A. (2008) Identification of adropin as a secreted factor linking dietary macronutrient intake with energy homeostasis and lipid metabolism. *Cell Metab.* **8,** 468–481
2. Ganesh Kumar, K., Zhang, J., Gao, S., Rossi, J., McGuinness, O. P., Halem, H. H., Culler, M. D., Mynatt, R. L., and Butler, A. A. (2012) Adropin deficiency is associated with increased adiposity and insulin resistance. *Obesity* **20,** 1394–1402
3. Lovren, F., Pan, Y., Quan, A., Singh, K. K., Shukla, P. C., Gupta, M., Al-Omran, M., Teoh, H., and Verma, S. (2010) Adropin is a novel regulator of endothelial function. *Circulation* **122,** S185–S192
4. Aydin, S., Kuloglu, T., and Aydin, S. (2013) Copeptin, adropin and irisin concentrations in breast milk and plasma of healthy women and those with gestational diabetes mellitus. *Peptides* **47,** 66–70
5. Butler, A. A., Tam, C. S., Stanhope, K. L., Wolfe, B. M., Ali, M. R., O'Keeffe, M., St-Onge, M. P., Ravussin, E., and Havel, P. J. (2012) Low circulating adropin concentrations with obesity and aging correlate with risk factors for metabolic disease and increase after gastric bypass surgery in humans. *J. Clin. Endocrinol. Metab.* **97,** 3783–3791
6. Celik, A., Balin, M., Kobat, M. A., Erdem, K., Baydas, A., Bulut, M., Altas, Y., Aydin, S., and Aydin, S. (2013) Deficiency of a new protein associated with cardiac syndrome X called adropin. *Cardiovasc. Ther.* **31,** 174–178
7. Celik, E., Yilmaz, E., Celik, O., Ulas, M., Turkcuoglu, I., Karaer, A., Simsek, Y., Minareci, Y., and Aydin, S. (2013) Maternal and fetal adropin levels in gestational diabetes mellitus. *J. Perinat. Med.* **41,** 375–380
8. Gozal, D., Kheirandish-Gozal, L., Bhattacharjee, R., Molero-Ramirez, H., Tan, H. L., and Bandla, H. P. (2013) Circulating adropin concentrations in pediatric obstructive sleep apnea: potential relevance to endothelial function. *J. Pediatr.* **163,** 1122–1126
9. Lian, W., Gu, X., Qin, Y., and Zheng, X. (2011) Elevated plasma levels of adropin in heart failure patients. *Intern. Med.* **50,** 1523–1527
10. Qiu, X., He, J. R., Zhao, M. G., Kuang, Y. S., Xu, S. Q., Zhang, H. Z., Hu, S. P., Chen, J., and Xia, H. M. (2014) Relationship between human cord blood adropin levels and fetal growth. *Peptides* **52,** 19–22
11. Sayin, O., Tokgoz, Y., and Arslan, N. (2014) Investigation of adropin and leptin levels in pediatric obesity-related nonalcoholic fatty liver disease. *J. Pediatr. Endocrinol. Metab.* **27,** 479–484
12. St-Onge, M. P., Shechter, A., Shlisky, J., Tam, C. S., Gao, S., Ravussin, E., and Butler, A. A. (2014) Fasting plasma adropin concentrations correlate with fat consumption in human females. *Obesity* **22,** 1056–1063
13. Topuz, M., Celik, A., Aslantas, T., Demir, A. K., Aydin, S., and Aydin, S. (2013) Plasma adropin levels predict endothelial dysfunction like flow-mediated dilatation in patients with type 2 diabetes mellitus. *J. Investig. Med.* **61,** 1161–1164
14. Wu, L., Fang, J., Chen, L., Zhao, Z., Luo, Y., Lin, C., and Fan, L. (2014) Low serum adropin is associated with coronary atherosclerosis in type 2 diabetic and non-diabetic patients. *Clin. Chem. Lab. Med.* **52,** 751–758
15. Kapushesky, M., Emam, I., Holloway, E., Kurnosov, P., Zorin, A., Malone, J., Rustici, G., Williams, E., Parkinson, H., and Brazma, A. (2010) Gene Expression Atlas at the European Bioinformatics Institute. *Nucleic Acids Res.* **38,** D690–D698
16. Xu, A., Lam, M. C., Chan, K. W., Wang, Y., Zhang, J., Hoo, R. L., Xu, J. Y., Chen, B., Chow, W. S., Tso, A. W., and Lam, K. S. (2005) Angiopoietin-like protein 4 decreases blood glucose and improves glucose tolerance but induces hyperlipidemia and hepatic steatosis in mice. *Proc. Natl. Acad. Sci. U.S.A.* **102,** 6086–6091
17. Hui, X., Zhu, W., Wang, Y., Lam, K. S., Zhang, J., Wu, D., Kraegen, E. W., Li, Y., and Xu, A. (2009) Major urinary protein-1 increases energy expenditure and improves glucose intolerance through enhancing mitochondrial function in skeletal muscle of diabetic mice. *J. Biol. Chem.* **284,** 14050–14057
18. Zhang, X., Xu, A., Chung, S. K., Cresser, J. H., Sweeney, G., Wong, R. L., Lin, A., and Lam, K. S. (2011) Selective inactivation of c-Jun NH2-terminal kinase in adipose tissue protects against diet-induced obesity and improves insulin sensitivity in both liver and skeletal muscle in mice. *Diabetes* **60,** 486–495
19. Law, I. K., Xu, A., Lam, K. S., Berger, T., Mak, T. W., Vanhoutte, P. M., Liu, J. T., Sweeney, G., Zhou, M., Yang, B., and Wang, Y. (2010) Lipocalin-2 deficiency attenuates insulin resistance associated with aging and obesity. *Diabetes* **59,** 872–882
20. Käll, L., Krogh, A., and Sonnhammer, E. L. (2007) Advantages of combined transmembrane topology and signal peptide prediction: the Phobius web server. *Nucleic Acids Res.* **35,** W429–W432
21. Petersen, T. N., Brunak, S., von Heijne, G., and Nielsen, H. (2011) SignalP 4.0: discriminating signal peptides from transmembrane regions. *Nat. Methods* **8,** 785–786
22. Nielsen, H., and Krogh, A. (1998) Prediction of signal peptides and signal anchors by a hidden Markov model. *Proc. Int. Conf. Intell. Syst. Mol. Biol.* **6,** 122–130
23. Krogh, A., Larsson, B., von Heijne, G., and Sonnhammer, E. L. (2001) Predicting transmembrane protein topology with a hidden Markov model: application to complete genomes. *J. Mol. Biol.* **305,** 567–580
24. Xu, A., Wang, Y., Keshaw, H., Xu, L. Y., Lam, K. S., and Cooper, G. J. (2003) The fat-derived hormone adiponectin alleviates alcoholic and nonalcoholic fatty liver diseases in mice. *J. Clin. Invest.* **112,** 91–100
25. Takeda, Y., Akasaka, K., Lee, S., Kobayashi, S., Kawano, H., Murayama, S., Takahashi, N., Hashimoto, K., Kano, M., Asano, M., Sudo, K., Iwakura, Y., and Watanabe, K. (2003) Impaired motor coordination in mice lacking neural recognition molecule NB-3 of the contactin/F3 subgroup. *J. Neurobiol.* **56,** 252–265
26. Bizzoca, A., Virgintino, D., Lorusso, L., Buttiglione, M., Yoshida, L., Polizzi, A., Tattoli, M., Cagiano, R., Rossi, F., Kozlov, S., Furley, A., and Gennarini, G. (2003) Transgenic mice expressing F3/contactin from the TAG-1 promoter exhibit developmentally regulated changes in the differentiation of cerebellar neurons. *Development* **130,** 29–43
27. Sakurai, K., Toyoshima, M., Ueda, H., Matsubara, K., Takeda, Y., Karagogeos, D., Shimoda, Y., and Watanabe, K. (2009) Contribution of the neural cell recognition molecule NB-3 to synapse formation between parallel fibers and Purkinje cells in mouse. *Dev. Neurobiol.* **69,** 811–824
28. Cui, X. Y., Hu, Q. D., Tekaya, M., Shimoda, Y., Ang, B. T., Nie, D. Y., Sun, L., Hu, W. P., Karsak, M., Duka, T., Takeda, Y., Ou, L. Y., Dawe, G. S., Yu, F. G., Ahmed, S., Jin, L. H., Schachner, M., Watanabe, K., Arsenijevic, Y., and Xiao, Z. C. (2004) NB-3/Notch1 pathway via Deltex1 promotes neural progenitor cell differentiation into oligodendrocytes. *J. Biol. Chem.* **279,** 25858–25865
29. Hu, Q. D., Ma, Q. H., Gennarini, G., and Xiao, Z. C. (2006) Cross-talk between F3/contactin and Notch at axoglial interface: a role in oligodendrocyte development. *Dev. Neurosci.* **28,** 25–33
30. Medof, M. E., Nagarajan, S., and Tykocinski, M. L. (1996) Cell-surface

engineering with GPI-anchored proteins. *FASEB J.* **10,** 574–586
31. Lerman, I., Harrison, B. C., Freeman, K., Hewett, T. E., Allen, D. L., Robbins, J., and Leinwand, L. A. (2002) Genetic variability in forced and voluntary endurance exercise performance in seven inbred mouse strains. *J. Appl. Physiol.* **92,** 2245–2255
32. Klein, S. M., Vykoukal, J., Lechler, P., Zeitler, K., Gehmert, S., Schreml, S., Alt, E., Bogdahn, U., and Prantl, L. (2012) Noninvasive *in vivo* assessment of muscle impairment in the mdx mouse model: a comparison of two common wire hanging methods with two different results. *J. Neurosci. Methods* **203,** 292–297
33. Sakurai, K., Toyoshima, M., Takeda, Y., Shimoda, Y., and Watanabe, K. (2010) Synaptic formation in subsets of glutamatergic terminals in the mouse hippocampal formation is affected by a deficiency in the neural cell recognition molecule NB-3. *Neurosci. Lett.* **473,** 102–106
34. Shimoda, Y., and Watanabe, K. (2009) Contactins: emerging key roles in the development and function of the nervous system. *Cell Adh. Migr.* **3,** 64–70
35. Imayoshi, I., and Kageyama, R. (2011) The role of Notch signaling in adult neurogenesis. *Mol. Neurobiol.* **44,** 7–12
36. Barski, J. J., Hartmann, J., Rose, C. R., Hoebeek, F., Mörl, K., Noll-Hussong, M., De Zeeuw, C. I., Konnerth, A., and Meyer, M. (2003) Calbindin in cerebellar Purkinje cells is a critical determinant of the precision of motor coordination. *J. Neurosci.* **23,** 3469–3477
37. Aydin, S., Kuloglu, T., Aydin, S., Eren, M. N., Yilmaz, M., Kalayci, M., Sahin, I., Kocaman, N., Citil, C., and Kendir, Y. (2013) Expression of adropin in rat brain, cerebellum, kidneys, heart, liver, and pancreas in streptozotocin-induced diabetes. *Mol. Cell Biochem.* **380,** 73–81
38. Bolte, S., and Cordelières, F. P. (2006) A guided tour into subcellular colocalization analysis in light microscopy. *J. Microsc.* **224,** 213–232